POLITECNICO
MILANO 1863

SCUOLA DI INGEGNERIA INDUSTRIALE
E DELL'INFORMAZIONE

Speed Control of a Separately Excited DC Motor in a Realistic Scenario

Dynamics of Electrical Machines and Drives

Automation and Control Engineering

Lazzaro Francesco, 11095668

Academic year: 2024-2025

Summary

1. Introduction

In the case under consideration a tramway vehicle must move in a 10 km pathway with slope variations, following requirements on speed. The tram is powered by 4 Separately Excited DC electric motors.

Distance [km]	Slope [%]	Speed
0 – 1	0	$v_r/2$
1 - 3	0	v_r
3 - 4	5	v_r
4 - 6	0	v_{max}
6 - 8	0	v_r
8 - 9	-5	v_r
9 - 10	0	$v_r/2$

Table 1: Road features.

The parameters v_r and v_{max} are the speeds reached by the vehicle when operating at rated and maximum speed of the DC motors respectively. The other specifications needed in the report are now presented.

- Line Voltage $V_l = 600\ V$
- Rated Power of each motor $P_e = 21\ kW$
- Motor Rated Speed $v_r = 970\ rpm$
- Tramway Maximum Speed $v_{max} = 42\ \ km/h$
- Overall Rated Current $I_n = 156\ A$
- Torque Constant $K_s = 1.06\ Nm/A^2$
- Armature Resistance $R_a = 0.39\ \Omega$
- Armature Circuit Time Constant $\tau_a = 10\ ms$
- Excitation Circuit Rated Voltage $V_{en} = 60\ V$
- Excitation Circuit Rated Current $I_{en} = 5\ A$
- Excitation Resistance $R_e = 12\ \Omega$
- Excitation Time Constant $\tau_e = 0.1\ s$

Mechanical System:

- Tramway Mass $m_T = 15\ T = 15000\ kg$
- Regular Amount of People $n_t = 130\ people$
- Average Person Weight $w_t = 80\ kg$
- Friction Coefficient $\beta = 0.81\ Nms$
- Wheel Diameter $dw = 680\ mm$
- Gearbox Ratio $\rho = 13/74$

Equations (1) and (2), included in the exercise guidelines, were used respectively to convert the motor's angular velocity into the tram's linear speed, and to determine the equivalent inertia of the overall mechanical system.

$$v_{m/s} = \Omega_{rad/s} \cdot \rho \cdot \frac{d_w}{2} \tag{1}$$

$$J_{eq} = m \cdot \frac{v_m^2}{\Omega_{\frac{rad}{s}}^2} = m \cdot \rho^2 \cdot \frac{d_w^2}{4} \tag{2}$$

The last requirement concerns the tramway's acceleration capability: it must be able to go from a complete stop to its top speed in no more than 25 seconds.

2. Preliminary Calculations

The next sections will walk through the preliminary calculations needed to define the remaining parameters and motion profiles essential for developing the speed control system discussed in this report. These elements play a key role in modeling the system's dynamics and shaping of a control strategy that fulfills the given performance criteria.

2.1. Total Mass and Equivalent Inertia

The system total mass is given by the sum of the tramway mass and total load.

$$m_{Total} = m_T + n_t \cdot w_t = 25.4\,T \tag{3}$$

By replacing the result in Eq. (4) the equivalent moment of inertia of the mechanical system can be calculated.

$$J_{eq} = m_{Total} \cdot \rho^2 \cdot \frac{d_w^2}{4} = 90.6181\ kg \cdot m^2 \tag{4}$$

2.2. Electrical Missing Quantities

With the available parameters, the inductances of the excitation and armature circuits can be found as follows.

$$L_a = R_a \cdot \tau_a = 3.9\ mH \tag{5}$$

$$L_e = R_e \cdot \tau_e = 1.2\ H \tag{6}$$

The nominal back electromotive force (EMF) is computed using two distinct expressions, Equations (7) and (8), because they apply to different motor operating conditions and are both necessary for accurately modeling standard and high-speed behavior.

Equation (7) is used in the motor's regular operating region, where the back EMF is proportional to the angular speed and the excitation flux. In this regime, the flux is considered constant, making the back EMF calculation straightforward and suitable for normal operation.

$$E_n = v_l - R_a \cdot I_n = 539.16\,V \tag{7}$$

Equation (8), on the other hand, is applied when the motor operates in the flux weakening region, typically beyond its nominal speed. In this case, the excitation current i_e is intentionally reduced to lower the excitation flux $\psi_{ae}(i_e)$, which allows the motor to spin faster without exceeding the drive's voltage limits. **This approach assumes that the flux $\boldsymbol{\psi_{ae}(i_e)}$, depends approximately linearly on $\boldsymbol{i_e}$, which simplifies both modeling and control.**

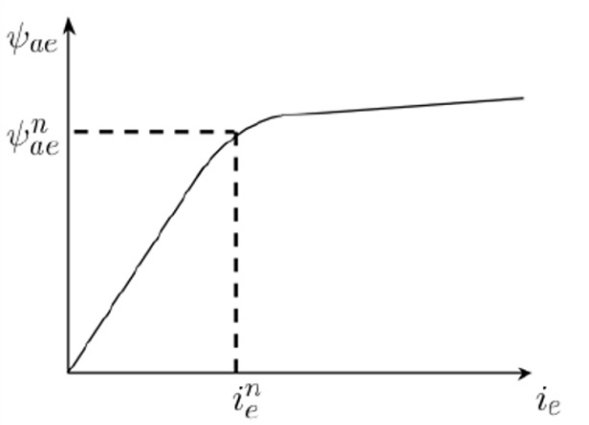

Figure 1: Linkage Flux and Excitation Current Relationship

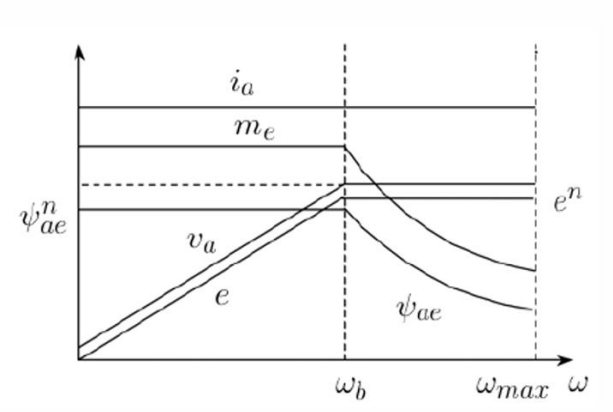

Figure 2: Operating Region

Equation (8) is obtained by evaluating at nominal conditions the equation that allows us to find the reference for the excitation current in the flux weakening region.

$$E_n = K_s \cdot i_{en} \cdot \Omega_r = 538.36\ V \tag{8}$$

2.3. Speed Reference Profile

The speed profiles of the tramway and the DC motors are obtained by converting the angular speed into the linear speed domains using Equation (1), as shown below.

$$v_{r_{tram}} = v_r \cdot \frac{2\pi}{60} \cdot \rho \cdot \frac{d_w \cdot 10^{-3}}{2} \cdot \frac{3600}{1000} = 21.8421\ km/h \tag{9}$$

$$v_{max_{motor}} = v_{max} \cdot \frac{1000}{3600} \cdot \frac{1}{\rho} \cdot \frac{2}{d_w \cdot 10^{-3}} = 195.3243\ rad/s \tag{10}$$

Then the maximum linear acceleration admissible for the system is calculated.

$$a_{max} = \frac{v_{max}}{25} = 0.467\ m/s^2 \tag{11}$$

The following figure shows the speed profile used as the reference signal Ω_{ref}, expressed both in terms of the tram's linear motion and the motor's rotational speed.

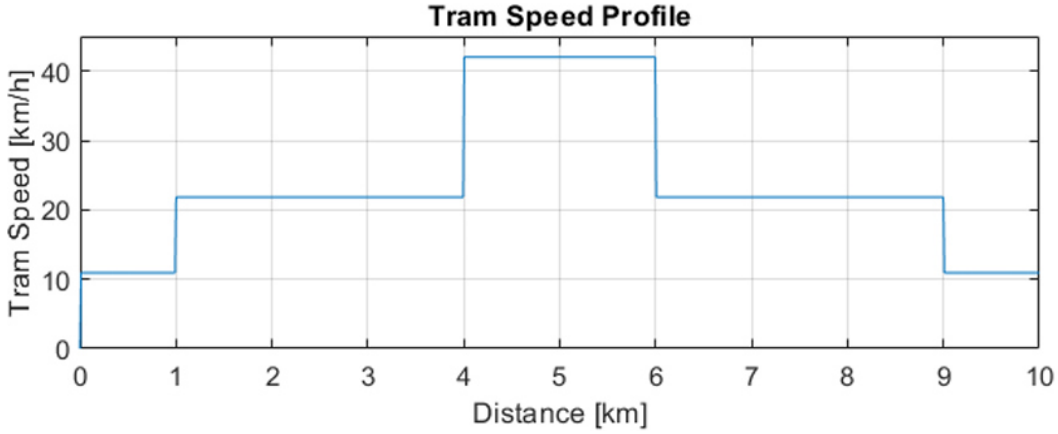

Figure 3: Reference Speed Profile for the tramway

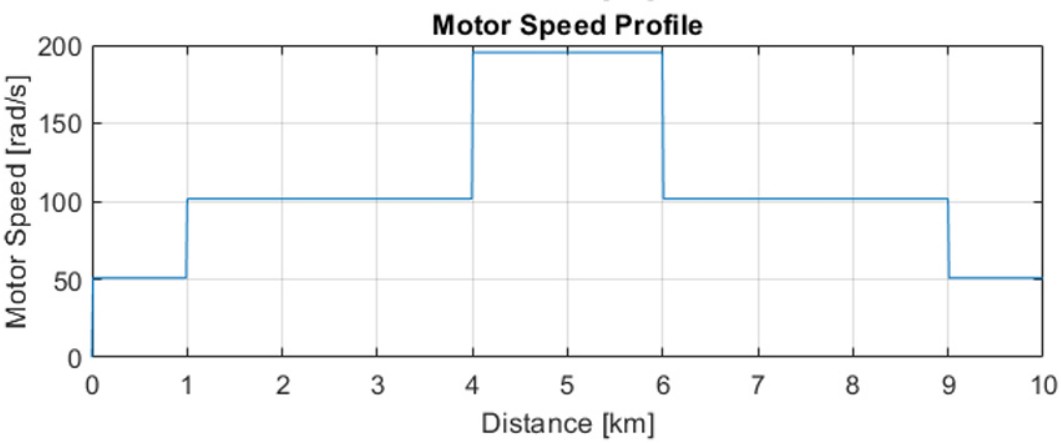

Figure 4: Reference Speed Profile for the Motor

2.4. Slope and Load Torque Profile

As mentioned in the project brief, both the path's slope and the load's required torque vary along the 10 km route. When the slope is uphill, the torque demand increases while when it's downhill, it decreases. To determine the load torque across these sections, Equation (12) is used.

$$T_l = 9.81 \cdot \rho \cdot m_{Total} \cdot \frac{d_w}{2} \cdot \sin^{-1}(slope)\ [Nm] \tag{12}$$

The next figures represent the slope profile respect to the path and the required torque, accounting for the variation.

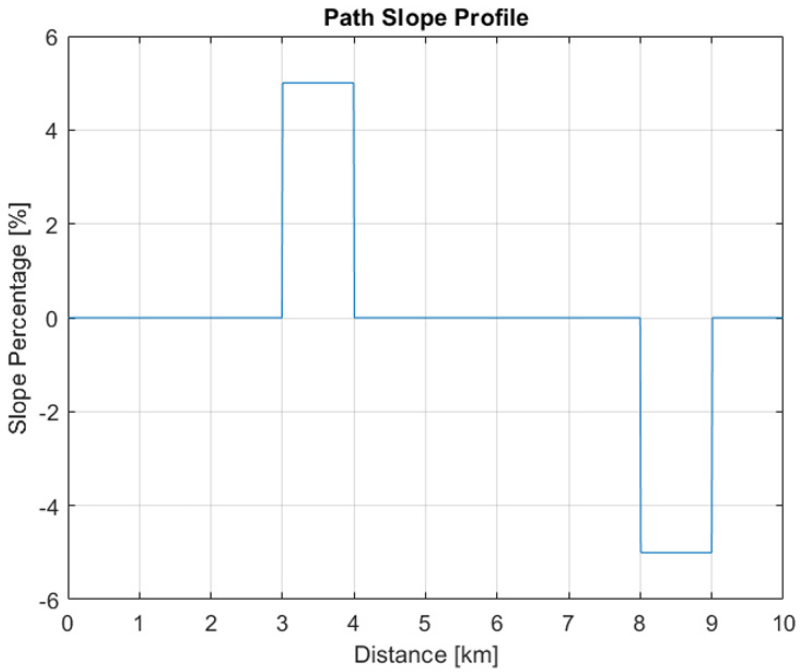

Figure 5: Slope Profile

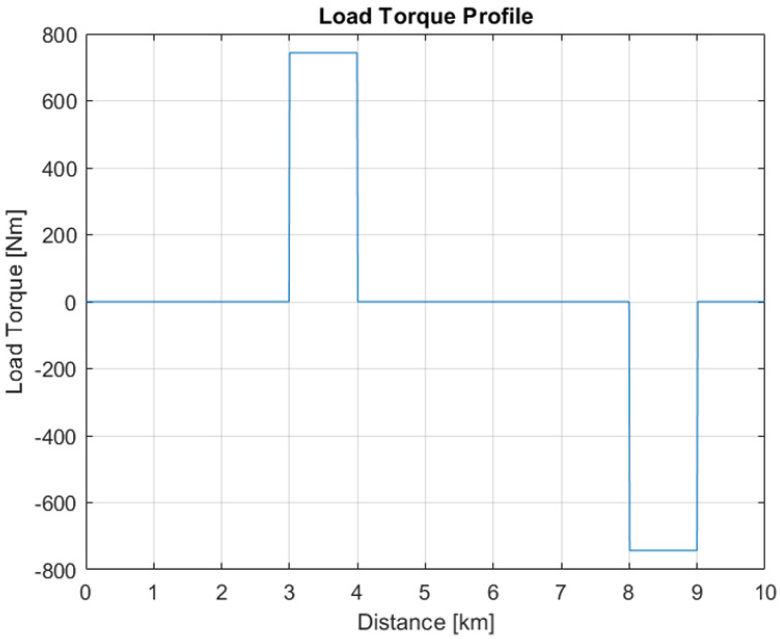

Figure 6: Load Torque Profile

3. Control System Design and Tuning

Speed control for a DC motor is typically handled using two PI controllers, one for the armature current and one for the motor speed. This setup works well as long as the motor stays within its rated speed. In this project, however, the motor is required to operate beyond that limit, which makes it necessary to also regulate the excitation current.

Since there were no specific performance goals, the control strategy was built using a standard approach. The torque is controlled through the armature current, which is preferred due to its faster dynamic response compared to the excitation current ($\tau_a \ll \tau_e$). The latter is only involved during flux weakening, when the motor exceeds its nominal speed (as previously shown in Figure 1 and 2).

The speed controller is tuned by following the common rule that the outer control loop should be significantly slower than the inner one. In this case, the speed loop is set to be slower than the armature current control loop by at least a 10 factor.

Given the considerations discussed earlier, Table 2 outlines the target specifications for each of the subsystem controllers. These values will guide the tuning of the PI controllers. Since the systems are already in minimal form and don't involve delays or unstable zeros, the crossover frequency is used as a practical reference to define their bandwidth.

Regulator	Crossover Freq. [rad/s]	Phase Margin [°]
Armature Current $\boldsymbol{i_a}$	40	90
Excitation Current $\boldsymbol{i_e}$	30	90
Speed $\boldsymbol{\Omega_m}$	4	90

Table 2: Regulators Parameters

3.1. Armature Current Regulator

The development of the armature current regulator is achieved using the ***pidtune*** MATLB tool, employing the equation (13) and the parameters of the previous table.

$$G_{i_a} = \frac{I_a}{V_a} = \frac{1}{R_a + s \cdot L_a} = \frac{1}{0.39 + s \cdot 3.9 \cdot 10^{-3}} \tag{13}$$

The crossover frequency can be evaluated using the Bode diagram of the closed-loop system.

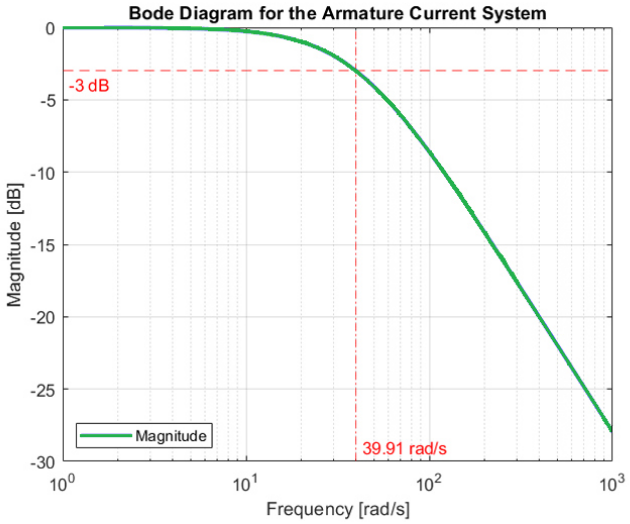

Figure 7: Armature Current Control System Bandwidth

The PI controller is implemented in Simulink using also the back calculation to include the antiwindup behavior. The results obtained are the following.

Parameter	Value
K_p	0.155
K_i	15.5
T_{PI}	0.01
ω_c [rad/s]	39.91

Table 3: Armature Current Regulator's Parameters

3.2. Excitation Current Regulator

The excitation current regulator was designed in the same way of the previous regulator, using the ***pidtune*** MATLB tool, employing the equation (14) and the parameters of table 2.

$$G_{i_e} = \frac{I_e}{V_e} = \frac{1}{R_e + s \cdot L_e} = \frac{1}{12 + s \cdot 1.2} \tag{14}$$

The crossover frequency can be evaluated using the Bode diagram of the closed-loop system.

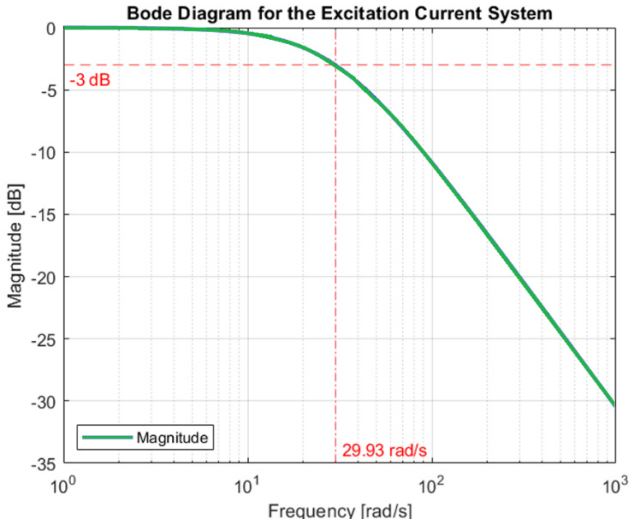

Figure 8: Excitation Current Control System Bandwidth

The PI controller is implemented in Simulink using also the back calculation to implement the antiwindup behavior. The results obtained are the following.

Parameter	Value
K_p	36.2
K_i	362
T_{PI}	0.1
ω_c [rad/s]	29.93

Table 4: Excitation Current Regulator's Parameters

3.3. Speed Regulator

In the first iteration, the speed regulator was tuned using the same approach as for the current ones, based on the system described in Equation (15). Although the initial performance was acceptable, the response showed a noticeable overshoot when reaching the maximum speed. To address this, the PI controller was then manually adjusted, and the final parameters used are listed in Table 5.

$$G_m = \frac{\Omega_m}{T} = \frac{1}{\beta + s \cdot J_{eq}} = \frac{1}{0.81 + s \cdot 90.62} \tag{15}$$

Parameter	Value
K_p	100
K_i	5
T_{PI}	20
ω_c	1.14
ω_ϕ	1.10
ϕ_m	87.87

Table 5: Speed Regulator's Parameters

For this analysis, the inner control loop, responsible for armature current, is assumed to behave as a unitary gain. This assumption holds, as the current loop is 20 times faster than the outer speed control loop. Since the speed regulator was manually tuned, the stability and robustness of the overall system were verified by analyzing the loop transfer function. The key indicators, such as phase margin and crossover frequency, are reported in the table above.

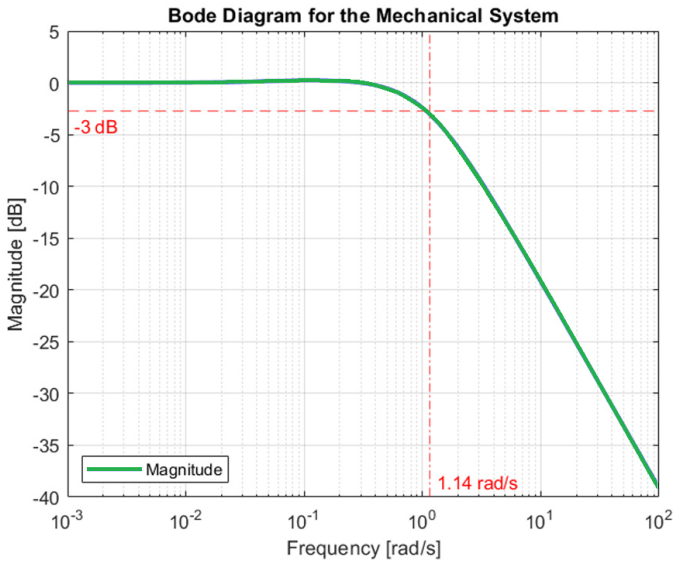

Figure 9: Mechanical System Bandwidth

4. Control Scheme Implementation

The Control Scheme is implemented in Simulink using a modular approach to better represent the different roles of each section.

4.1. Reference Signals Computation

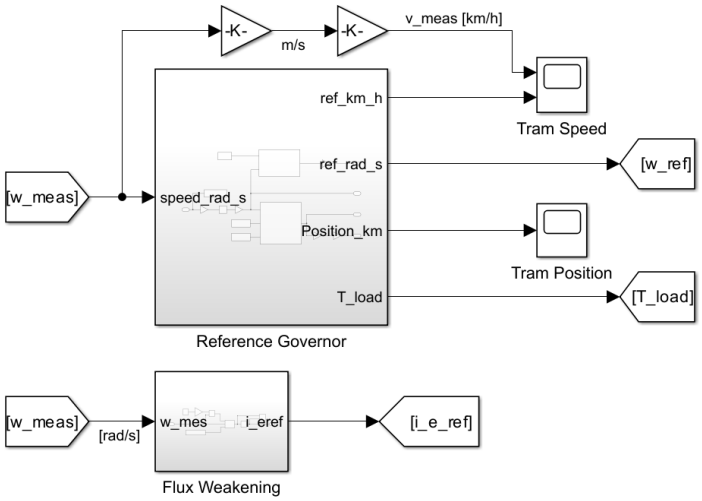

Figure 10: Reference Signals Computation Scheme

The reference governor subsystem generates the motion profiles shown in the previous chapters. This is achieved by integrating the speed signal to track the tram's position and implementing the logic using MATLAB Function blocks within Simulink.

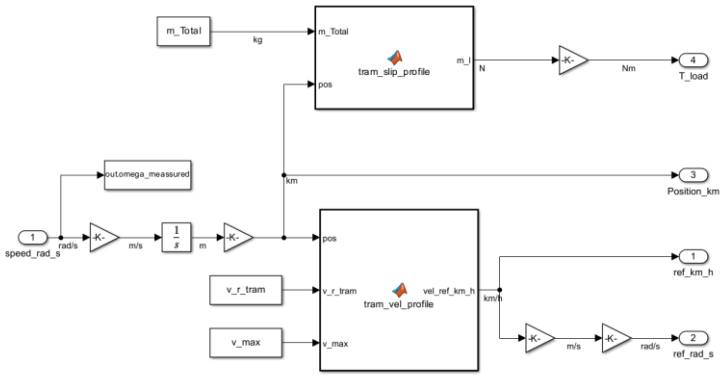

Figure 11: Reference Governor

In parallel, the Flux Weakening subsystem becomes active once the motor exceeds its rated speed, computing the appropriate excitation current reference to allow the system to operate safely and efficiently beyond nominal conditions.

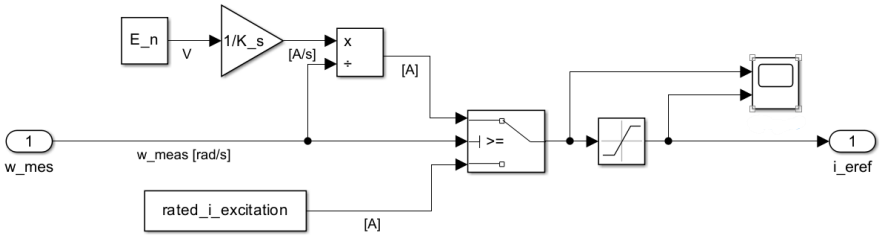

Figure 12: Flux Weakening

4.2. Dynamic Systems

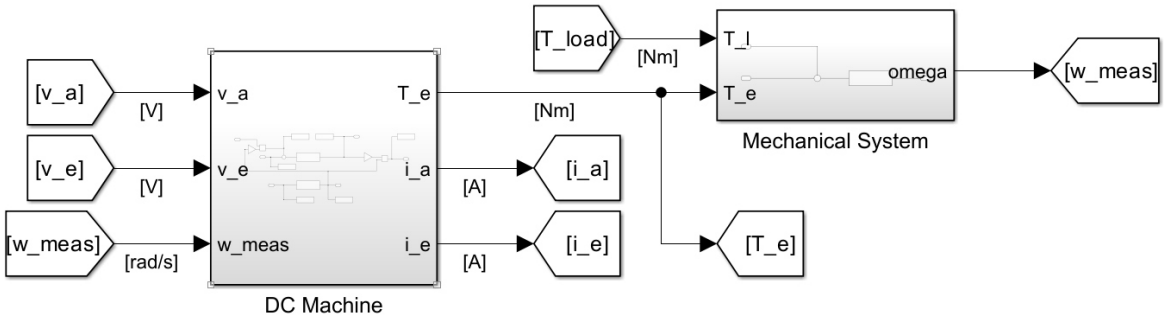

Figure 13: Dynamic Systems Scheme

The DC Machine subsystem includes the two models used in Sections 3.1 and 3.2 for tuning the PI controllers associated with the armature and excitation currents.

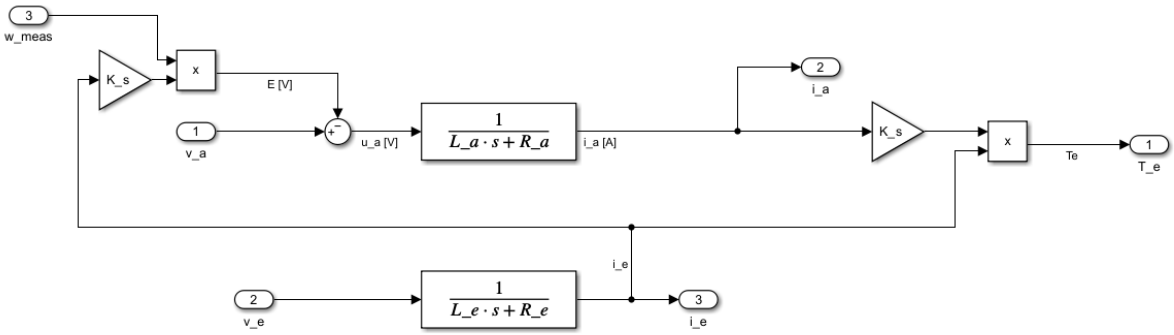

Figure 14: DC Machine Dynamics

Meanwhile, the Mechanical System implements the transfer function described in Equation (15), which was used as the basis for designing the speed controller.

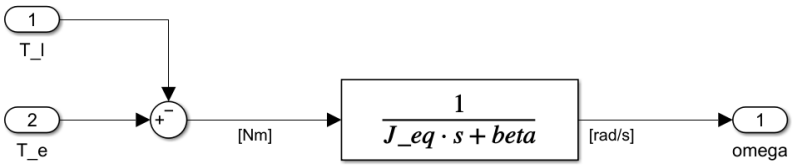

Figure 15: Mechanical System

4.3. Main Control Scheme

Initially, the armature current control is held off until the excitation circuit is active, since the magnetic field needs to be established first. Additionally, the rate at which the speed reference increases is limited according to the maximum acceleration identified earlier in the report. Lastly, the saturation limits of the PI controller for the armature current are not fixed but they are updated dynamically based on the value of the back EMF, which changes during operation.

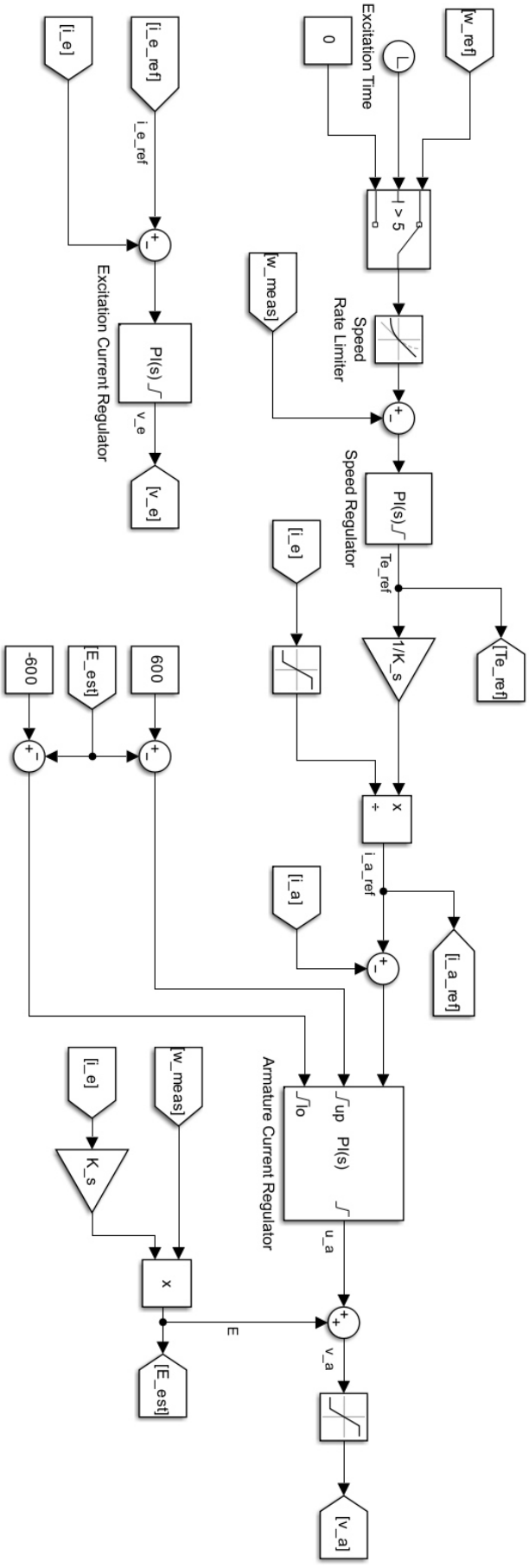

Figure 16: Main Control Scheme

4.4. Mechanical and Electrical Output Quantities

In this section are reported the Simulink schemes for the output quantities

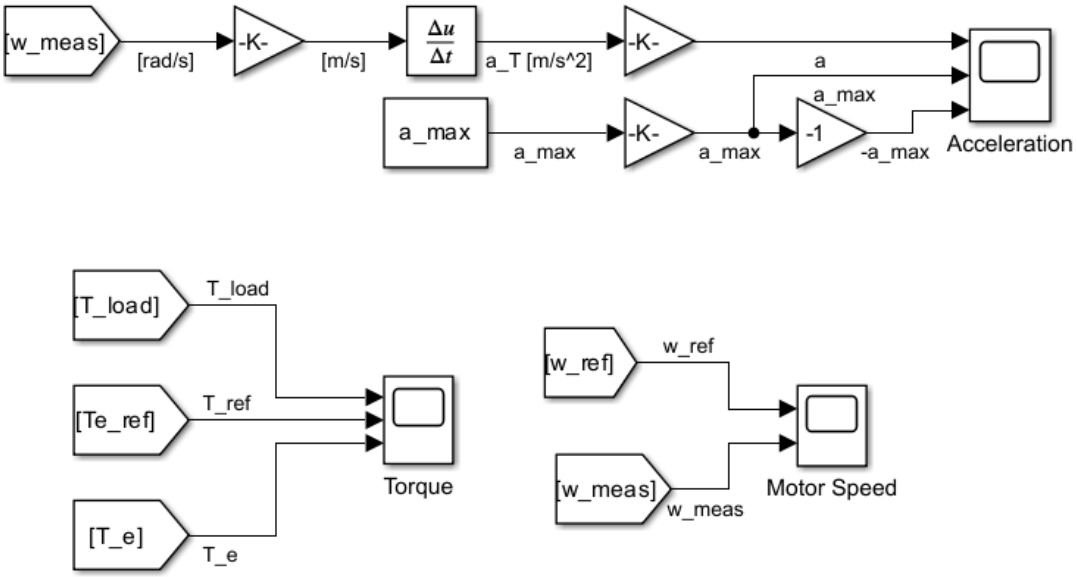

Figure 17: Mechanical Quantities

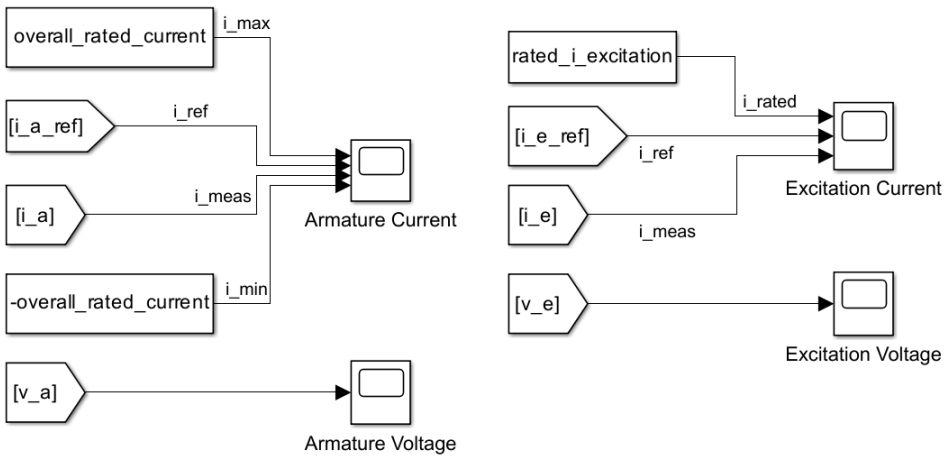

Figure 18: Electrical Quantities

5. Simulation Report

5.1. Acceleration Response

As for acceleration, the results are shown by comparing them to the project-defined limit. These thresholds, indicated by the red and blue lines, are slightly surpassed at a few points along the track, but are still acceptable. The acceleration constraint was intentionally introduced to add realism to the scenario, preventing unrealistically fast transitions between speed levels.

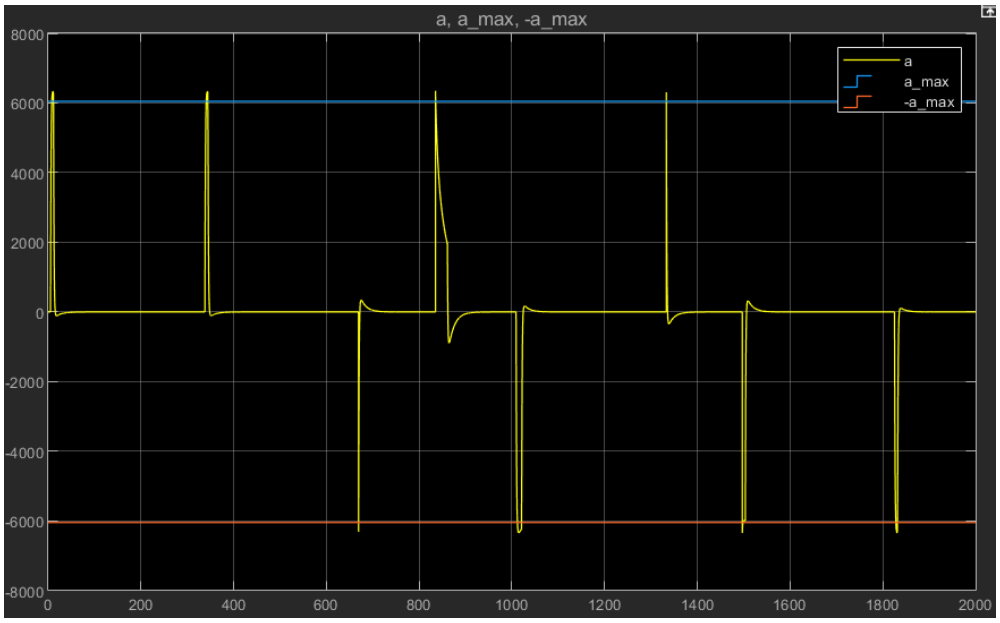

Figure 19: Acceleration Response

5.2. Speed Response

The simulation of the tram's speed controller confirmed that the speed profile was correctly implemented. The control system successfully tracked the reference with no steady-state error, thanks to the inclusion of an integrator in the loop. The overshoots observed at each change in the reference signal were anticipated, as they stem from the step transitions in the target speed.

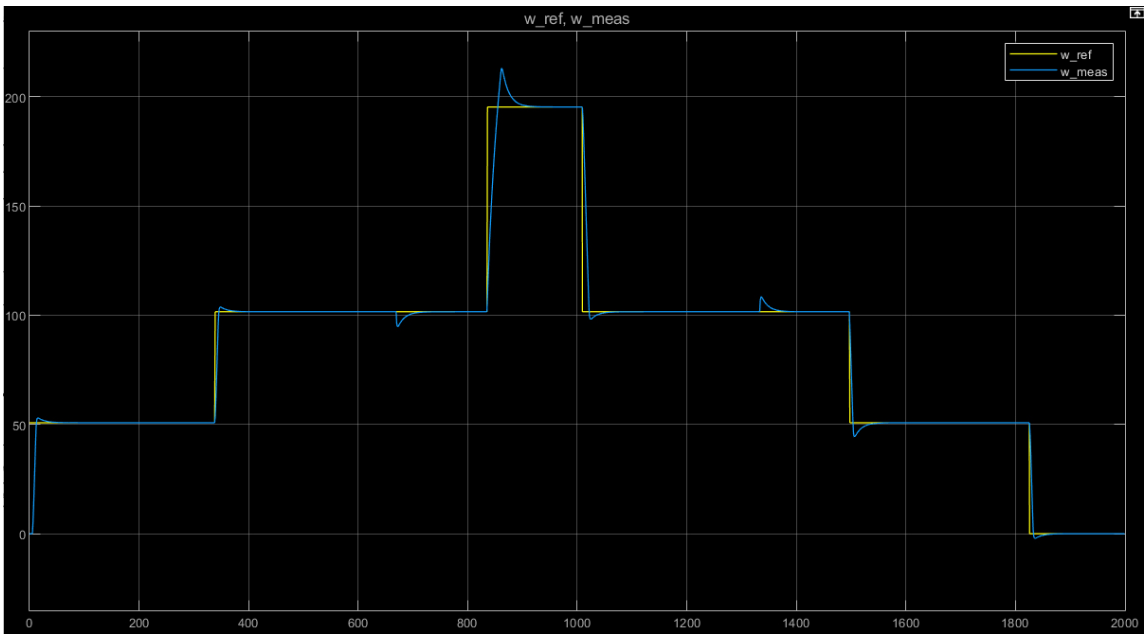

Figure 20: Speed Response

5.3. Excitation Current Response

Continuing with the performance evaluation, the simulation of the excitation current regulator reveals some key aspects. While the motor operates at speeds below its rated value, remaining in the constant torque region, the excitation current stays at its nominal level. This ensures optimal use of the motor's magnetic core, allowing it to perform efficiently in that range. When the motor speed goes above this threshold, even for a brief moment as seen during the overshoot, the excitation current reference drops immediately. This transition shifts the motor into the flux weakening region, which allows it to achieve higher speeds. The controller handles this change effectively. Thanks to its high bandwidth, it responds quickly and keeps the actual current closely aligned with the desired reference.

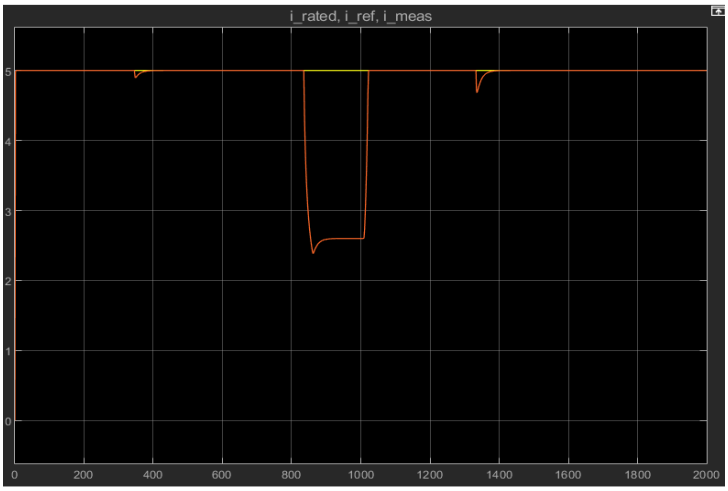

Figure 21: Excitation Current Response

5.4. Armature Current Response

The armature current response confirms that the controller operates effectively within the expected parameters. During operation below the rated speed, within the constant torque region, the current remains stable at its nominal value. However, when the speed reference undergoes a sudden increase such as during a slope variation the armature current exhibits a high transient overshoot. This response is consistent with the controller reacting to the sudden change in the speed demand, which requires increased torque and consequently higher current. Despite the reference current occasionally exceeding the system's available power, the actual current remains capped due to the implemented anti-windup mechanism in the controller.

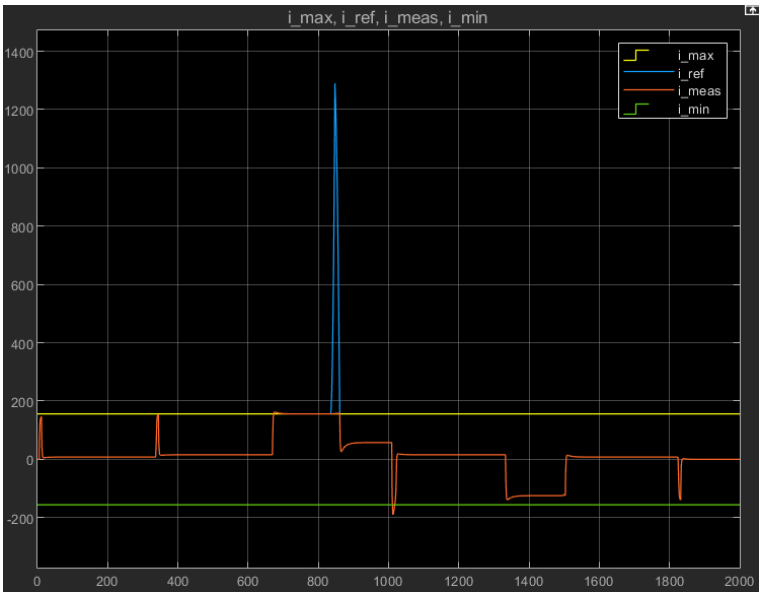

Figure 22: Armature Current Response

5.5. Torque Response

In the flux weakening region, the torque response aligns with theoretical expectations for this motor type. Although the armature current remains constant, a reduction in flux linkage causes a corresponding decrease in torque output. This behavior reflects the fundamental trade-off in the flux weakening operating region, where magnetic saturation limits the motor's ability to maintain torque despite a steady current. The observed torque drop illustrates the transition between the constant torque and flux weakening regimes, confirming that the motor and control strategy properly adapt to changing operating conditions.

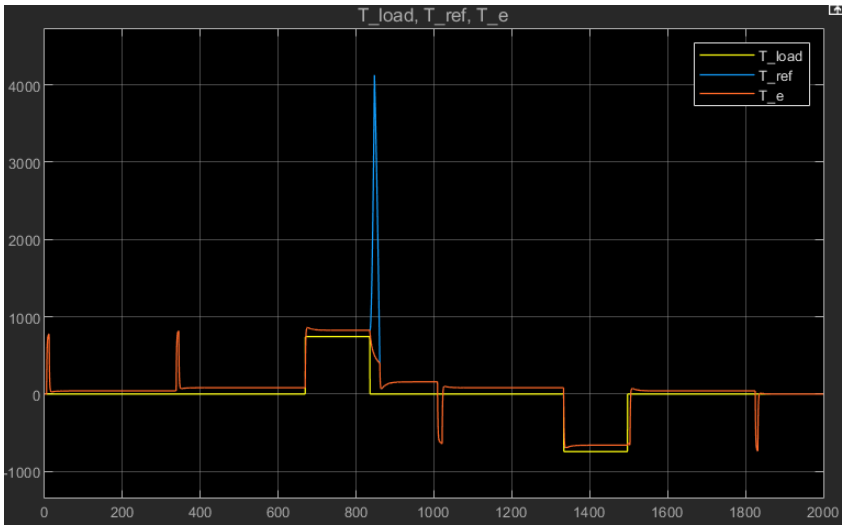

Figure 23: Torque Response

6. Final Discussion

This project successfully developed a control system for a tram powered by 4 SEDC motors, designed to accurately follow a speed profile over varying slopes. The controller architecture was carefully developed to achieve high performance while respecting bandwidth limitations and ensuring that inner-loop regulators could operate independently without complicating the design of the outer speed control loop.

By implementing a detailed mathematical model and performing extensive simulations, the control parameters were iteratively tuned to significantly reduce speed overshoot by approximately 50%. The results demonstrate robust and reliable performance across both transient and steady-state conditions, confirming the controller's effectiveness in handling even step changes in speed and load.

Furthermore, the motor operation remained consistently within prescribed operating regions throughout the simulation, respecting constraints related to temperature limits and magnetic material properties. This careful adherence ensures motor longevity and reliable operation under real-world scenario, validating the control strategy as a practical solution for tram motion control under complex dynamic scenarios.